AIAA 82-4163

Extension of Local Momentum Theory to Hovering Rotor with Distorted Wake

Keiji Kawachi*
University of Tokyo, Tokyo, Japan

The local momentum theory is extended in this paper to include the effects of a rotor wake deformation in hovering flight. A comparison of this extended local momentum theory with a prescribed wake vortex theory is presented. The results indicate that the extended local momentum theory has the capability of achieving a level of accuracy similar to that of the prescribed wake vortex theory, using a much smaller amount of computer time. It is also shown that the analytical results obtained using either theory are in reasonable agreement with experimental data.

Nomenclature

AR = aspect ratio of a blade
a = lift curve slope, rad^{-1}
a_s = speed of sound
b = number of blades
C = attenuation coefficient
C_T = thrust coefficient $= T/\rho\pi R^2(R\Omega)^2$
c = blade chord
i = running index or inclination angle of tip path plane (positive forward tilt)
(i,j,k) = coordinate of a blade element
j = running index
K = parameters showing tip vortex positions
l = airloading
(l,m) = coordinate of a local station on rotor rotational plane
M = Mach number
M_{tip} = Mach number of blade tip
$\dot{m}$ = mass of air associated with local momentum given by Eq. (2)
n = number of spanwise partitions
P = position of tip vortex
R = rotor radius
r = radial position
r_β = flapping hinge offset
T = thrust
t = time
U = horizontal inflow velocity of a blade element given by Eq. (2)
u = induced velocity given by using simple vortex model
V = forward velocity
V_N = normal component of inflow velocity (positive downward)
v = induced velocity (positive downward)
x = nondimensional radial position $= r/R$
$x_{i,c}$ = nondimensional radial position given by Eq. (2)
x_T = nondimensional radial position of tip vortex given by Eq. (4)
x_β = nondimensional flapping hinge offset $= r_\beta/R$
Z = distance from rotor rotational plane (positive downward)
z_T = nondimensional axial position of tip vortex given by Eq. (5)
Δ = small increment
δ_{lm} = function
θ = blade pitch angle (positive leading-edge up) $= \theta_{0.75} + \theta_t(x-0.75) + \theta_{1c}\cos\psi + \theta_{1s}\sin\psi + \ldots$
θ_t = blade twist rate
$\theta_{0.75}$ = collective pitch angle at $x = 0.75$
λ = running index
ρ = air density
Σ = summation
σ = solidity $= bc/\pi R$
ϕ = inflow angle or wake age
ψ = azimuth angle
Ω = rotor rotational speed

Subscripts and Superscripts

b = number of blades
i = spanwise partition, quantity of ith hypothetical wing, or quantity of ith tip vortex
j = azimuth-wise or time-wise partition
k = quantity of kth blade
λ = azimuth-wise or time-wise partition, or spanwise position
0 = uniform or initial value
$1c$, $1s$ = first harmonic contents of Fourier cosine and sine series
$(\ )^j_{lm}$ = quantity at a local station (l, m) at time $t = j$

Introduction

IT has been pointed out that a wake deformation has strong effects on the airloading and induced velocity distribution of a helicopter rotor in hovering flight.[1-4] There are two methods commonly used to analyze these wake deformation effects, free wake vortex theory[5] and prescribed wake vortex theory.[1-4] In free wake vortex theory, each of the vortex segments moves with the corresponding local induced velocity; therefore, this theory does not require any experimental data for wake positions. The theory, however, requires an enormous amount of computer time, and the calculation may be difficult because of instability of the vortex elements. In prescribed wake vortex theory, the vortex segments are positioned as observed in experiments. This theory is more practical and the calculation is not difficult; however, even prescribed wake vortex theory requires considerable computer time.

The local momentum theory is based on the instantaneous balance between the fluid momentum and the blade elemental lift at a local station in the rotor rotational plane.[6-8] The theory has the capability of evaluating effectively time-wise variations of airloading and induced velocity distributions along a helicopter blade span. The theory previously assumed that the wake of a hovering rotor did not move in the radial

Received Oct. 2, 1981; revision received Feb. 11, 1982.

*Associate Professor, Institute of Interdisciplinary Research, Faculty of Engineering; previously, National Research Council Associate, NASA Ames Research Center, Moffett Field, Calif.

direction; therefore, the theory gave almost the same result as the rigid wake vortex theory.

In order to analyze those effects of the wake deformation of a hovering rotor more effectively, the local momentum theory is extended. In the new distorted wake model to be described in this paper, fluid elements surrounding a rotor are located as observed in experiments. In addition, the model to calculate the attenuation coefficient is improved in order to include the effect of the blade tip vortex. The spanwise lift distributions obtained by this extended local momentum theory are compared with experimental results and with those of a prescribed wake vortex theory.[3,4]

Local Momentum Theory

The local momentum theory is briefly explained here in order to obtain necessary concepts to understand the distorted wake model presented in this paper. More detailed explanations of the local momentum theory are given in Refs. 6-9. In the local momentum theory, a rotor blade is assumed to be operating in a sheared flow in the rotor rotational plane. The rotor rotational plane is assumed to be divided into small elements called local stations. The position of each local station is given by the coordinates (l,m). The rotor blade moves past these local stations, and leaves an induced velocity at each of the local stations (Fig. 1). The rotor blade is represented by a series of hypothetical wings of decreasing wing span (Fig. 2). Each hypothetical wing has an elliptical circulation along its wing span. The trailing vortices shed from this hypothetical wing are straight, perpendicular to the wing span and extended to infinity; therefore, the induced velocity is uniform along the span of each hypothetical wing. Momentum theory is used to obtain the relation between the lift distribution and the induced velocity distribution for each hypothetical wing. The actual airloading and induced velocity distribution of a real rotor blade is represented by the summation of the lift and induced velocity of this series of hypothetical wings. Therefore, the lift per unit span, l_i, acting on a local segment of the real rotor blade spanned by (x_i,x_{i+1}), is calculated by using momentum theory. The upwash velocities outside of the hypothetical wings are neglected, when calculating the induced velocity distribution inside of the real rotor blade.[6] This is because the upwash region outside of each hypothetical wing is limited to an area near the wing tip.

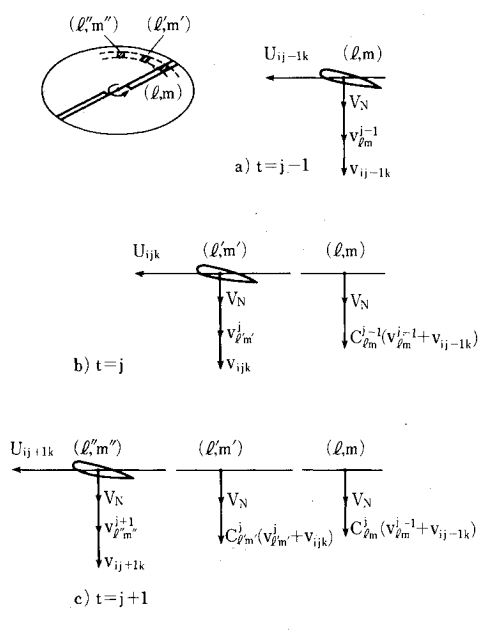

Fig. 1 Time-wise variation of induced velocity on rotor rotational plane.

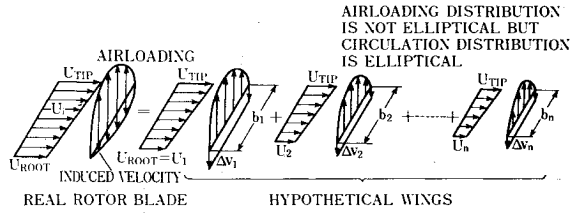

Fig. 2 Decomposition of a rotor blade to hypothetical wings.[6]

Equating this lift per unit span from momentum theory with that from blade element theory, the following equations are obtained:

$$l_i=\int_{x_i}^{x_{i+1}}\frac{\tfrac{1}{2}\rho U_i^2 c_i a_i(\theta_i-\phi_i)\,dx}{(x_{i+1}-x_i)}=\sum_{\lambda=1}^{i}2\tilde{m}_\lambda\Delta v_\lambda \qquad (1)$$

where

$$U_i=V\sin\psi_j+R\Omega x_{i,c}$$

$$\tilde{m}_\lambda=\int_{x_i}^{x_{i+1}}\rho R(1-x_\lambda)(\Omega Rx+V\sin\psi_j)\sqrt{1-\left(\frac{2x-1-x_\lambda}{1-x_\lambda}\right)^2}\times\frac{dx}{(x_{i+1}-x_i)}$$

$$x_{i,c}=(x_i+x_{i+1})/2 \qquad \psi_j=\psi_{k,0}+\sum_{\lambda=1}^{j}\Delta\psi_\lambda$$

$$\phi_i=(V\sin i+v_{lm}^{j}+v_{ijk})/U_i \qquad \Delta v_i=v_{ijk}-v_{i-1jk} \qquad (2)$$

In the above equations, c_i, θ_i and a_i are a blade chord, a pitch angle, and a lift curve slope of the blade element at $x=x_{i,c}$, respectively. $\psi_{k,0}$ and $\Delta\psi$ are the initial azimuth angle of the kth blade and the azimuth-wise increment of each step of the numerical calculation. The induced velocity is separated into the following two components: v_{ijk},† the induced velocity generated by the blade element under consideration at time $t=j$; and v_{lm}^{j}, the entire remaining induced velocity generated by blade elements that have previously passed through the local station (l,m). Only the first component, v_{ijk}, is related to the lift when momentum balance is considered [Eqs. (1) and (2)]. If v_{lm}^{j} is given, the induced velocity distribution, v_{ijk}, is calculated from Eqs. (1) and (2).

The time-wise variation of induced velocity is given by using "attenuation coefficients." The induced velocity at a local station (l,m), where a blade element is just passing through at time $t=j-1$, is given as $v_{ij-1k}+v_{lm}^{j-1}$ (Fig. 1). After a small time interval has passed, the blade element moves to station (l',m'). The disturbed air at station (l,m) has gone downward and the field in the rotor rotational plane is partially filled with fresh air. Therefore, the induced velocity at station (l,m) has been changed at time $t=j$. By introducing this time-wise changing rate of the induced velocity, the remaining induced velocity, v_{lm}^{j}, at station (l,m) at time $t=j$ can be related to the previous induced velocity as follows:

$$v_{lm}^{j}=C_{lm}^{j-1}\left(v_{lm}^{j-1}+\sum_{i=1}^{n}\sum_{k=1}^{b}v_{ij-1k}\cdot\delta_{lm}\right) \qquad (3)$$

†Generally, the first subscript of any quantity, i, indicates the ith radial segment of the blade, the second subscript, j, indicates the time or azimuthal location of the blade segment, and the third subscript, k, indicates the kth blade of a b-bladed rotor.

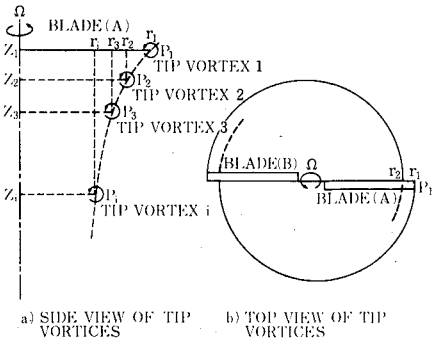

Fig. 3 Views of tip vortices.

where δ_{lm} is one if any blade element exists at station (l,m) at time $t=j-1$, and otherwise it is zero. The time-wise rate of change of the induced velocity, C_{lm}^{j-1}, is called the "attenuation coefficient." The value of the attenuation coefficient is determined by experiments or by analytical calculation based on an infinite vortex cylinder.[7,9]

In summary, the total calculation procedure of the local momentum theory is as follows:

1) Assume initial value of the induced velocity, v_{lm}^{0}.

2) Calculate induced velocity, v_{ijk}, and lift distribution, l_i, by using Eqs. (1) and (2).

3) Calculate attenuation coefficient, C_{lm}^{j}, by using the model of infinite vortex cylinder.

4) Calculate the remaining induced velocity at time $t=j+1$, v_{lm}^{j+1}, by using Eq. (3).

5) Repeat steps 2-4 for each time step.

New Hovering Model Including the Wake Deformation

The wake deformation of a hovering rotor is separated into spanwise deformation and axial deformation. The spanwise wake deformation includes the contraction and rollup of the vortices. The axial wake deformation is the axial deviation from the rigid helical wake position. In the local momentum theory, the spanwise wake deformation is equivalent to the spanwise movement of a local station on the rotor rotational plane. In order to express the axial wake deformation, a new model which would give a corresponding attenuation coefficient was developed. Because the effect of the tip vortex on a spanwise lift distribution is dominant among all the wake components, the model of the present theory was developed primarily to trace the behavior of the tip vortex. Figures 3a and 3b show the side view and top view of the tip vortex. Tip vortex 1 in Fig. 3a is shed from the blade under consideration (blade A) at position P_1 at time $t=j$. Tip vortex 2 was shed from the preceding blade (blade B) at position P_1 at time $t=j-1$, and is located at position P_2 at time $t=j$. The period between $t=j-1$ and $t=j$ is the period during which two neighboring blades successively pass through the same position of the rotor rotational plane; that is, $\Delta t_b=2\pi/b\Omega$. During the period Δt_b, tip vortex 2 moves from P_1 to P_2. Following the motion of tip vortex 2, a station on the rotor rotational plane moves from r_1 to r_2 during this period, where r_1 and r_2 are radial positions of tip vortices 1 and 2. Similarly, each station moves from r_{i-1} to r_i during the period following the motion of the ith tip vortex. The positions of the tip vortices are given by a generalized wake model[1-3,10]:

$$x_T=K_4+(1-K_4)e^{-K_3\phi} \tag{4}$$

$$z_T=K_1\phi \qquad 0\leqq\phi<(2\pi/b)$$

$$=K_1(2\pi/b)+K_2(\phi-2\pi/b) \qquad (2\pi/b)\leqq\phi \tag{5}$$

where x_T and z_T are the axial and radial nondimensional positions of the tip vortices. Using Eq. (4), the radial position

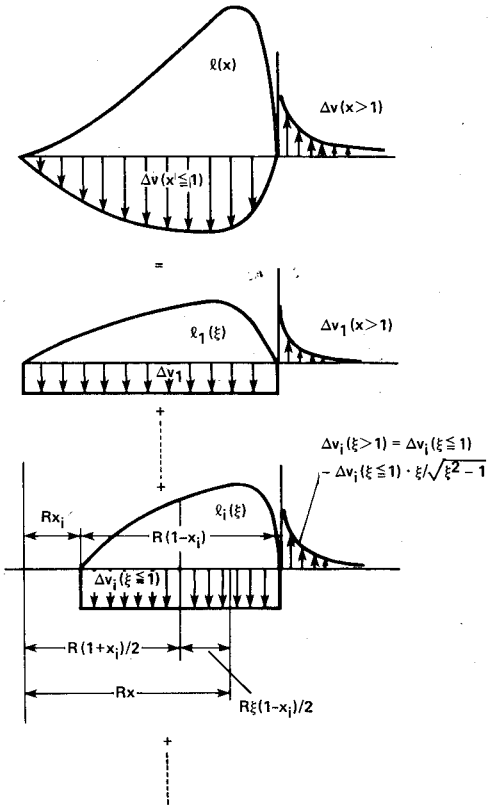

Fig. 4 Summation of induced velocity distributions of hypothetical wings.[6]

of the ith tip vortex is given as

$$r_i=R\{K_4+(1-K_4)e^{-K_3\phi_i}\} \tag{6}$$

$$\phi_i=(2\pi/b)(i-1) \tag{7}$$

Outside the rotor disk; $(r>R)$, each of the stations moves a distance equal to that between r_1 and r_2 toward the blade root in order to avoid making a gap between neighboring stations. At the inner area of the rotor $(r\leqq RK_4)$, the stations do not move, because no tip vortex moves into this area [Eq. (4)]. Therefore, the positions of the stations in the inner area are coincident with those of the rigid wake model. The parameters K_1, K_2, K_3 and K_4 in Eqs. (4-6) are determined by experimental data using flow visualization techniques. There are three available generalized wake models, one proposed by Landgrebe,[1] one by Kocurek and Tangler,[2] and one by Kocurek, Berkowitz and Harris.[10] In this paper, the second model is most frequently used because of its applicability over wide range variations of rotor geometry, and because of the convenience of comparison with other computer codes.

In the local momentum theory, the real rotor blade is represented by a series of hypothetical wings. Each hypothetical wing is one-sidedly arranged (Fig. 2); therefore, when summing up induced velocities of the hypothetical wings, upwashes are not concentrated but distributed inboard of the blade tip $(x\leqq 1)$. Each upwash outside a hypothetical wing is limited to an area near the wing tip. These make it possible to neglect the upwashes inboard of the blade tip when calculating the induced velocity distribution of the rotor blade [Eqs. (1) and (2)]. The upwashes of the hypothetical wings are, however, concentrated outboard of the blade tip as shown in Fig. 4. Although the effect of each upwash outside a hypothetical wing is small, this concentration brings that the summation of upwashes outboard of the preceding blade tip is sometimes strong enough to give an effect on the lift distribution of the following blade. Because each station moves in this distorted wake model, a part of the following

blade (the hatched area in Fig. 3b) operates in the upwash region generated by the preceding blade, even in the hovering case. Consequently, it is necessary to calculate the upwash distribution outside the blade tip, whereas the upwashes inboard of the blade tip are neglected.

Remembering the calculation procedure to obtain the value of the induced velocity of each hypothetical wing, i.e., Δv_i, it is necessary to omit the upwash only inboard of the blade tip ($x \leqq 1$). This is due to the fact that in the one-sided arrangement the angle of attack at any spanwise station of the blade is independent of the tip-side upwash, unlike the inboard upwash. Therefore, after the value of the induced velocity, Δv_i, is determined by omitting the upwash inboard of the blade tip ($x \leqq 1$), it is a simple matter to estimate the upwash outboard of the blade tip ($x > 1$) as follows:

$$v_{ijk}(x_i > 1) = \sum_{\lambda=1}^{n} \Delta v_\lambda \left(1 - \frac{2x_i - 1 - x_\lambda}{2\sqrt{(x_i - 1)(x_i - x_\lambda)}}\right) \tag{8}$$

Thus, the downwash distribution along the blade is calculated by using Eqs. (1) and (2), and the upwash distribution outboard of the blade tip is given by Eq. (8). Furthermore, in Eq. (3), the induced velocity v_{lm}^j at a station (l,m) should be given by the summation of all velocities induced, not only those induced by the real blade elements ($x \leqq 1$, or $i \leqq n$) passing through the station, but also those induced by the hypothetical blade elements ($x > 1$, or $i > n$) extending through the tip-side upwash region. In addition to this, similar to the downwash, the time-wise variation of the upwash is expressed by using the attenuation coefficient. Consequently, in this case, Eq. (3) becomes

$$v_{lm}^j = C_{lm}^{j-1}\left(v_{lm}^{j-1} + \sum_{i=1}^{n'} \sum_{k=1}^{b} v_{ij-1k} \cdot \delta_{lm}\right) \tag{9}$$

where n' is the number of the spanwise partitions of the real and hypothetical blade. δ_{lm} should be considered to be one if any real or hypothetical blade element exists at the station (l,m) at time $t=j-1$; otherwise it should be considered to be zero.

The new model was also developed to take the wake deformation into account and to obtain the attenuation coefficient, C_{lm}^j, at the upwash region. Figure 5 shows the new model which is composed of a vortex ring and a semi-infinite vortex cylinder. The vortex ring represents the tip vortex nearest the rotor rotational plane, and the vortex cylinder represents the remaining tip vortices. The vortex cylinder is made of the continuous vortex, the strength of which is equal to that of the axially averaged tip vortices.[11] The strength of the vortex ring is equal to that of the tip vortex. Figure 5a shows that the preceding blade passes through a local station at time $t=j-1$. The vortex ring is located on the rotor rotational plane, and the top of the vortex cylinder is located at the position of the second tip vortex. The distance between the top of the vortex cylinder and the rotor rotational plane is Z_2. Figure 5b shows that the following blade comes just

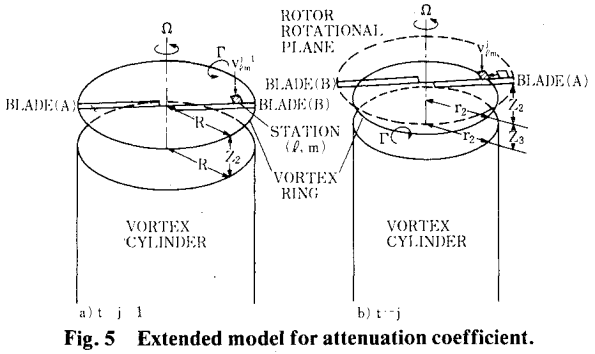

Fig. 5 Extended model for attenuation coefficient.

before the station at time $t=j$. During the period between time $t=j-1$ and $t=j$, the vortex ring and the vortex cylinder move downward and radially contract. Using Eq. (5), the vertical position Z_i is given by

$$\begin{aligned} Z_i &= RK_1\phi_i && i \leqq 2 \\ &= R\{K_1(2\pi/b) + K_2(\phi_i - 2\pi/b)\} && i > 2 \end{aligned} \tag{10}$$

where ϕ_i is given by Eq. (7). The radius of the vortex ring is equal to that of the tip vortex nearest to the rotor rotational plane (Fig. 5b). For simplicity, the radius of the vortex cylinder is assumed to be equal to that of the vortex ring instead of the corresponding tip vortex radius. This leads, however, to an overestimation of the radius of the vortex cylinder because of the contraction of the tip vortices as shown in Fig. 3a. The radii of the vortex ring and the vortex cylinder are given as Eq. (6).

The attenuation coefficient is defined by the rate of change of induced velocities at a station (l, m) between time $t=j$ and $t=j-1$. In the present model including the wake deformation, the station (l,m) moves from position r_{i-1} to position r_i on the rotor rotational plane during this period. Consequently, the attenuation coefficient of that station is given as

$$C_{lm}^{j-1} = u_{lm}^j / u_{lm}^{j-1} \tag{11}$$

where u_{lm}^{j-1} is the induced velocity at position r_{i-1} on the rotor rotational plane at time $t=j-1$, and u_{lm}^j is the induced velocity at position r_i on the rotor rotational plane at time $t=j$. Because the station at the inner part of the blade ($r \leqq RK_4$) does not move, the attenuation coefficient of that station is given as the rate of change of the induced velocities at the same radial position between time $t=j$ and $t=j-1$. The stations which are located between positions r_2 and R at time $t=j$ were situated outside the rotor disk ($r > R$) at time $t=j-1$. Therefore, when determining the attenuation coefficients of these stations by using Eq. (11), the induced velocity u_{lm}^{j-1} is calculated outside the rotor disk. If the old model presented in Refs. 7 and 9, which is composed of the vortex cylinder alone, is used, the induced velocity u_{lm}^{j-1} is zero outside the rotor disk, and it is impossible to define the attenuation coefficients of these stations. Consequently, the discrete vortex was introduced into the present model.

In the Landgrebe wake model and in the Kocurek and Tangler wake model, the parameters K_1, K_2 and K_3 in Eqs. (4-6) and (10) are functions of a thrust coefficient.[1,2] In the present method, those parameters are calculated at each time step by using the value of a thrust coefficient. There is an analytical solution[11] for the induced velocity around the vortex cylinder or the vortex ring. Based on this solution, general tables of the induced velocity are constructed for the vortex ring and for the vortex cylinder, before the start of the calculation. The induced velocities, u_{lm}^j and u_{lm}^{j-1}, are obtained from these general tables, and the attenuation coefficient is calculated at each time step by using Eq. (11). The entire calculation is completed when the thrust coefficient reaches a steady state. The calculation procedure of the present theory is shown by Fig. 6.

Results and Discussions

A comprehensive study has been conducted to check the extended local momentum theory. The spanwise lift distributions for five different rotors were calculated by the new theory. The results were compared with experimental data and with those obtained by using other analyses. Table 1 shows the geometrical characteristics and the operating conditions of the rotors considered in this study (see also

Refs. 12-16). Three of them are model rotors, and two are full scale rotors.

Two computer codes of the prescribed wake vortex theory were used in this study, the AMI lifting surface program,[4] and the UTRC lifting line program.[3] In the present theory and the UTRC code, the lift curve slope of airfoil sections is given as

$$a = a_0/\sqrt{1-M^2} \tag{12}$$

$$a_0 = 6.05\ (1/\text{rad}) \tag{13}$$

M is the Mach number of the airfoil section, and it is given as

$$M = \Omega R x_i / a_s \tag{14}$$

where a_s is the speed of sound. The above equations are based on Refs. 17 and 18. Because the angles of attack of the airfoil sections are far below the stall angles in all experimental cases selected in this study, the foregoing simple relations are applicable.

The sample results are shown in Figs. 7-11. Comparisons of the present theory with the AMI code, with the UTRC code, and with the first experiment[12] (case A) when using the Landgrebe wake model are presented in Fig. 7. The experimental result was obtained using a laser velocimeter to measure the bound circulation. The result obtained by using the present theory shows good correlation with that of the AMI code or of the UTRC code. The experimental data show a higher lift peak at the blade tip than the three theoretical estimations. This is probably caused by the existence of a larger wake deformation than estimated using the generalized wake model,[19] rather than by modeling errors in the three calculation models. In addition to these results, an analysis using the earlier rigid wake model of the local momentum theory is shown in Fig. 7. The lift curve slope of the airfoil section is taken as given by Eqs. (12-14). It is apparent that the extended local momentum theory improves the estimation of the lift distribution near the blade tip. Analyses of the same experiment (case A) when using the Kocurek and Tangler wake model are presented in Ref. 9, and are similar to the present results using the Landgrebe wake model.

An analysis of the second experiment (case B) using the Landgrebe wake model is shown in Fig. 8. The experimental data were measured in flight using an H-34 rotor (Table 4 in Ref. 13). Although the correlation between the present theory and the AMI code is not as good as the first experimental case shown in Fig. 7, it is reasonable. The results of the UTRC code are obtained using the collective pitch input mode and the thrust coefficient input mode. The result of the collective pitch input mode, in which the measured value of the collective pitch is used in the computer program, is shown by the double chain line. The result of the thrust coefficient input mode, in which the value of the thrust coefficient is used in the computer program, is shown by the broken line. When using the collective pitch input mode, the difference between the results of the AMI code and of the UTRC code is larger than the difference between the results of the AMI code and of the present theory. The thrust coefficient input mode gives better correlation, but a measurable difference between the AMI code and the UTRC code still exists near the blade tip. Because the same thrust coefficient is used in the AMI code and in the UTRC code when using the thrust coefficient input mode, the difference between these two results is caused by the difference between lifting surface and lifting line methods as well as by the difference between the numerical methods to calculate the thrust coefficient. In this experiment, the tip vortices generated by the preceding blade are closer to the

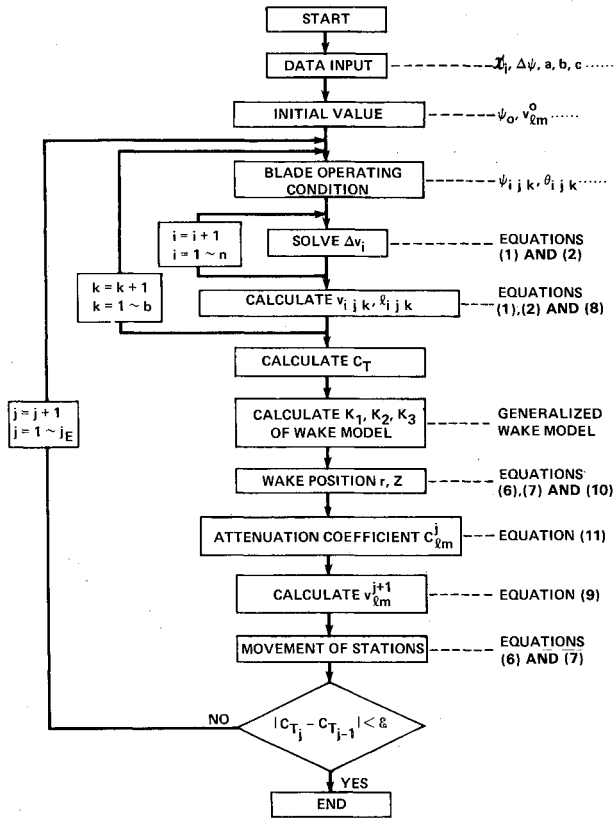

Fig. 6 Global flow chart of distorted wake model of local momentum theory.

Table 1 Rotor parameters and operating conditions

Case	A	B	C	D	E
Blade section	0012	0012	0012	0015	0012
Blade twist, θ_t, deg	−10.902	−8.0	−12.0	0	0
Collective pitch angle at $x=0.75$, $\theta_{0.75}$, deg	9.8	9.41	8.97	8.0	5.3
Rotor radius, R, m	1.045	8.53	6.67	0.762	2.32
Number of blades, b	2	4	2	2	2
Solidity, σ	0.0464	0.0621	0.0369	0.0637	0.0974
Aspect ratio of a blade, AR	13.7	20.5	17.3	10.0	6.54
Flapping hinge offset, x_β	0	0.0357	0	0	0
Mach number of blade tip, M_{tip}	0.226	0.583	0.639	0.188	0.360
Source	NASA TM 78615[12]	NASA TM X-952[13]	TCREC-TR-62-42[14]	NACA TN 2953[15]	NACA TN 3688[16]
	Model	H-34 flight test	UH-1A flight test	Model	Model

following blade than in the first experiment shown in Fig. 7. Therefore, the airloading distribution is more sensitive to the tip vortex positions which depend on the thrust coefficient. This is the primary reason for the poor correlation between the AMI code and the UTRC code when using the collective pitch input mode.

The results of the third experiment (case C), analyzed by the Kocurek and Tangler wake model, are shown in Fig. 9. The experimental data were obtained on a UH-1A helicopter.[14] The correlation between the present theory and the AMI code is very good. The correlation between the experiment and either the present theory or the AMI code is good. It is also apparent that the present extension of the local momentum theory demonstrates an improvement in the capability of estimating the lift distribution. In addition, the result using blade element theory with a uniform induced velocity is shown by the double chain line. The uniform induced velocity is given as $v_0 = \Omega R\sqrt{C_T/2}$ where the thrust coefficient is equal to that of the AMI code. The lift curve slope of the airfoil section in blade element theory is as given by Eqs. (12-14).

The analyses of the fourth experiment[15] (case D) using the Kocurek and Tangler wake model are presented in Fig. 10. The double chain line shows the result of the present theory when using the collective pitch input mode. This result is very similar to that of the AMI code obtained by using the collective pitch input mode. The experimental data, however, show poor correlation with the present theory when using the collective pitch input mode. Ironically, the previous rigid wake model gives better correlation with the experiment in this input mode. When using the thrust coefficient input mode, the present theory and the AMI code show good correlation with the experiment. The airloading distribution near the blade tip can be estimated only when using the distorted wake model.

The fifth experiment[16] (case E) was analyzed using the Kocurek and Tangler wake model. The results using the collective pitch input mode and the thrust coefficient input

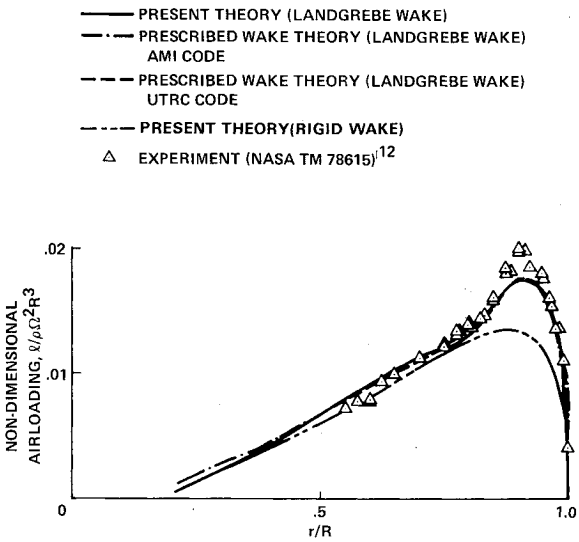

Fig. 7 Comparison of measured and calculated spanwise lift distributions in hover, with Landgrebe wake model ($b=2$, $\theta_t=-10.9$ deg, $\mathcal{R}=13.7$, $\theta_{0.75}=9.8$ deg).

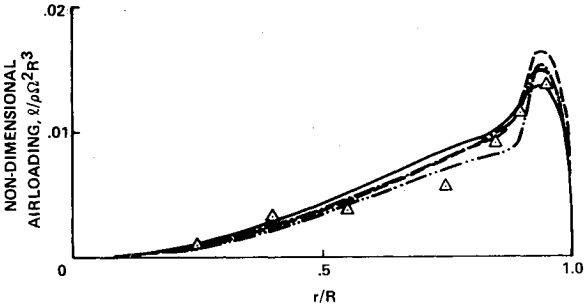

Fig. 8 Comparison of measured and calculated spanwise lift distributions in hover, with Landgrebe wake model ($b=4$, $\theta_t=-8.0$ deg, $\mathcal{R}=20.5$).

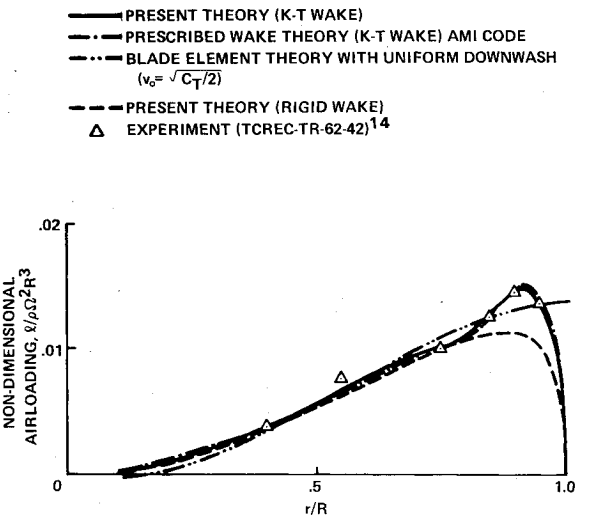

Fig. 9 Comparison of measured and calculated spanwise lift distributions in hover, with Kocurek and Tangler wake model ($b=2$, $\theta_t=-12.0$ deg, $\mathcal{R}=17.3$, $\theta_{0.75}=8.97$ deg).

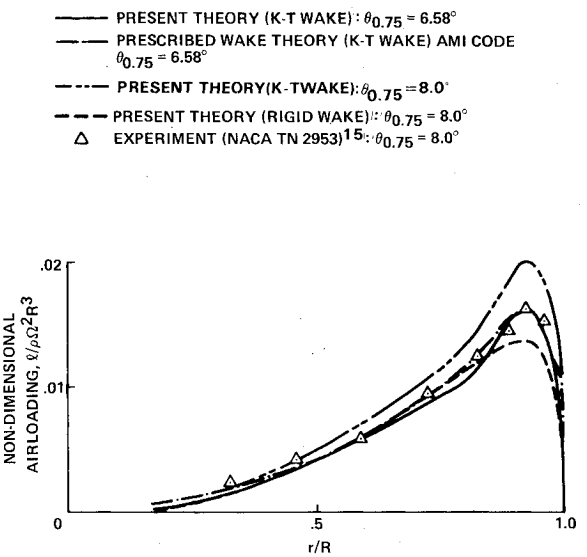

Fig. 10 Comparison of measured and calculated spanwise lift distributions in hover, with Kocurek and Tangler wake model ($b=2$, $\theta_t=0.0$ deg, $\mathcal{R}=10.0$).

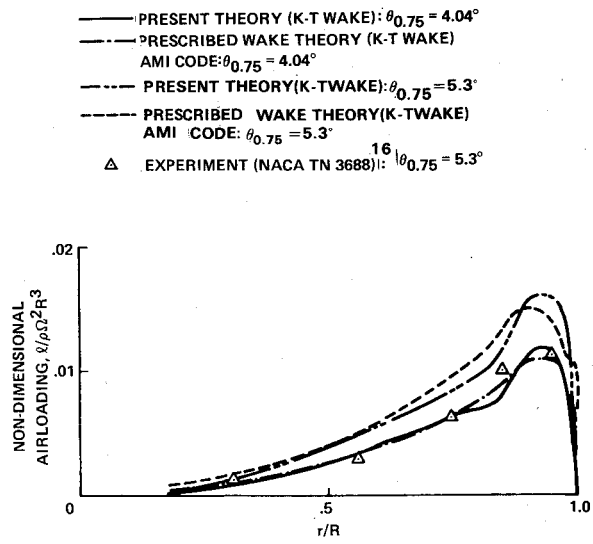

Fig. 11 Comparison of measured and calculated spanwise lift distributions in hover, with Kocurek and Tangler wake model ($b=2$, $\theta_t=0.0$ deg, $\mathcal{R}=6.54$).

mode are shown in Fig. 11. Again, only the thrust coefficient input mode of the present theory or of the AMI code shows good correlation with the experiment. The correlation between the present theory and the AMI code is reasonable in both input modes.

Reviewing analyses of the five experimental cases, correlation between the present theory and the AMI code is always good. However, the correlation near the blade tip is not as good as that of the inner part of the blade, nor is it as good when the aspect ratio of the blade becomes smaller, or when the tip vortices of the preceding blade are closer to the blade under consideration. These trends are due to the simplicity of the present model. An improved attenuation coefficient in the upwash region might be effective in obtaining better correlation.

The difference between the results obtained using the AMI code and the UTRC code is sometimes greater than the difference between those obtained using the AMI code and the present theory. The experimental results fluctuate around the three theoretical results, and it is difficult to determine which computer code gives the best correlation with the experiments. Therefore, the development of a more complicated model of the present theory, which might make it possible to obtain a better correlation with the AMI code alone, is not necessary at present.

The experimental data of the fourth and the fifth cases are very different from the theoretical estimation obtained by the present theory or by the AMI code when using the collective pitch input mode. This may be due to elastic torsion deflection of the blade. When the thrust coefficient input mode is used, however, the results obtained from using the distorted wake model show the best correlation with the experiments. In the other three experimental cases, the results obtained using the present theory and the AMI code show reasonable correlations with experimental results, even when the collective pitch input mode is used.

The computer time required for each of the three codes to obtain the results shown in Figs. 7 and 8 is given in Table 2. These calculations were conducted under the same condition by using CDC-7600 at Ames Research Center, NASA Moffett Field, Calif. The variation of the computer time of the UTRC code in the case of Fig. 8 is due to the difference of the convergence speeds of the iteration included in this code. The computer time required by the present theory is less than 1/15 of that of the UTRC code, and less than 1/60 of that of the AMI code.

Table 2 Comparison of computer time

	Computer time, s	
Code/case	Fig. 7	Fig. 8
Present theory	0.34	0.44
AMI code	23.18	43.03
UTRC code	6.37[a]	7.02-40.52[a]

[a] By the private letter, this UTRC code is the earlier version. The current CCHAP (Circulation Coupled Hover Analysis Program), which includes the UTRC lifting line method, requires approximately 2 seconds per case.

Conclusions

An extension of the local momentum theory to include the effect of the rotor wake contraction in hovering flight was presented. The extended local momentum theory was compared with a prescribed wake vortex theory. The results indicate that the extended local momentum theory has the capability of achieving a level of accuracy similar to that of the prescribed wake vortex theory over wide range variations of rotor geometrical parameters. It has also shown that the analytical results obtained using either theory were in reasonable agreement with experimental data. The computer time required by the present theory is less than 1/15 of that of the prescribed wake vortex theory. Consequently, this extended local momentum theory is especially effective when calculations are required for numerous cases.

Acknowledgments

Most of the work to extend the local momentum theory to the distorted wake model of hovering was conducted during the period of a National Research Council Resident Research Associateship, at NASA Ames Research Center. The author wishes to thank the following persons for their contributions to this paper: Professor Akira Azuma, University of Tokyo, Tokyo, Japan, from whom the author received the original idea of the extension of the theory; Dr. Wayne Johnson, Ames Research Center, who supported this study and provided valuable suggestions; and Mr. Henry Jones, also of the Ames Research Center, who provided assistance in the use of the AMI code and the UTRC code.

References

[1] Landgrebe, A.J., "The Wake Geometry of a Hovering Helicopter Rotor and Its Influence on Rotor Performance," *Journal of the American Helicopter Society*, Vol. 17, No. 4, Oct. 1972, pp. 3-15.

[2] Kocurek, J.D. and Tangler, J.L., "A Prescribed Wake Lifting Surface Hover Performance Analysis," *Journal of the American Helicopter Society*, Vol. 22, No. 1, Jan. 1977, pp. 24-35.

[3] Landgrebe, A.J., "An Analytical and Experimental Investigation of Helicopter Rotor Hover Performance and Wake Geometry Characteristics," Eustis Directorate, U.S. Army Air Mobility Research and Development Laboratory, Fort Eustis, Va., USAAMRDL TR 71-24, June 1971.

[4] Summa, J.M. and Clark, D.R., "A Lifting-Surface Method for Hover/Climb Airloads," *American Helicopter Society 35th Annual National Forum Proceedings*, May 1979.

[5] Clark, D.R. and Leiper, A.C., "The Free Wake Analysis—A Method for the Prediction of Helicopter Rotor Hovering Performance," *Journal of the American Helicopter Society*, Vol. 15, No. 1, Jan. 1970, pp. 3-11.

[6] Azuma, A. and Kawachi, K., "Local Momentum Theory and Its Application to the Rotary Wing," *Journal of Aircraft*, Vol. 16, No. 1, Jan. 1979, pp. 6-14.

[7] Azuma, A. and Kawachi, K., "Local Momentum Theory and Its Application to the Rotary Wing," AIAA Paper 75-865, June 1975.

[8] Stepniewski, W.Z., "Rotary-Wing Aerodynamics Vol. I—Basic Theories of Rotor Aerodynamics (with Application to Helicopters)," NASA CR-3082, 1979, pp. 219-230.

[9] Kawachi, K., "An Extension of the Local Momentum Theory to a Distorted Wake Model of a Hovering Rotor," NASA TM 81258, Feb. 1981.

[10] Kocurek, J.D., Berkowitz, L.F., and Harris, F.D., "Hover Performance Methodology at Bell Helicopter Textron," *American Helicopter Society 36th Annual National Forum Proceedings,* May 1980.

[11] Castles, W. Jr. and De Leeuw, J.H., "The Normal Component of the Induced Velocities in the Vicinity of a Lifting Rotor and Some Examples of Its Application," NACA Rept. 1184, 1954, (supersedes NACA TN 2912).

[12] Ballard, J.D., Orloff, K.L., and Luebs, A.B., "Effect of Tip Planform on Blade Loading Characteristics for a Two-Bladed Rotor in Hover," NASA TM 78615, Nov. 1979.

[13] Scheiman, J., "A Tabulation of Helicopter Rotor-Blade Difference Pressures, Stresses, and Motions as Measured in Flight," NASA TM X-952, 1964.

[14] "Measurement of Dynamic Air Loads on a Full-Scale Semirigid Rotor," Bell Helicopter Company, TCREC-TR-62-42, Dec. 1962.

[15] Meyer, J.R. Jr. and Falabella, G. Jr., "An Investigation of the Experimental Aerodynamic Loading on a Model Helicopter Rotor Blade," NACA TN 2953, 1953.

[16] Rabbott, J.P. Jr., "Static-Thrust Measurements of the Aerodynamic Loading on a Helicopter Rotor Blade," NACA TN 3688, July 1956.

[17] Lizak, A.A., "Two-Dimensional Wind Tunnel Tests on an H-34 Main Rotor Airfoil Section," U.S. Army Transportation Research Command, Fort Eustis, Va., TRECOM TR-60-53, 1960.

[18] Abbott, I.H. and Doenhoff, A.E., *Theory of Wing Sections,* Dover, N.Y., 1958.

[19] Johnson, W.R., "Comparison of Calculated and Measured Model Rotor Loading and Wake Geometry," NASA TM 81189, April 1980.